Quantifying carbon site switching dynamics in GaN by electron holography

K. Ji, M. Schnedler, Q. Lan, J.-F. Carlin, R. Butté, N. Grandjean, R. E. Dunin-Borkowski, And Ph. Ebert, and Ph. Ebert, Ernst Ruska-Centrum (ER-C-1), Forschungszentrum Jülich GmbH, 52425 Jülich, Germany

Institute of Physics, Ecole Polytechnique Fédérale de Lausanne, 1015 Lausanne, Switzerland

(Received 5 January 2024; accepted 29 January 2025; published 24 February 2025)

Off-axis electron holography is utilized to identify point defect reactions and quantify their dynamics by probing the time and temperature dependence of the Fermi level upon annealing. The methodology is illustrated using implanted carbon (C) in GaN, where a site switching phenomenon of C, from substitutional to interstitial, is found to be responsible for lifting the Fermi-level pinning in the lower part of the band gap. The carbon site switching process has an activation barrier energy of 2.27 ± 0.26 eV.

DOI: 10.1103/PhysRevResearch.7.013200

I. INTRODUCTION

Despite the persistent presence of carbon (C) during the metal-organic vapor phase epitaxy (MOVPE) of group-III nitride semiconductors and further device fabrication steps, the understanding of the role of carbon in electronic properties and long-term stability of nitride devices remains limited. On the one hand, C is believed to play a central role in the degradation processes of, e.g., laser diodes [1,2]. On the other hand, C is intentionally used to achieve semi-insulating layers, intended for reducing drain leakage currents and enhancing breakdown voltages in high-electron-mobility transistors (HEMTs) [3–7]. However, information about dynamic processes and point defect reactions to which C is subjected is scarce, although being of paramount importance to understand degradation as well as explore paths towards extended durability of group-III nitride devices.

The necessity for detailed investigations of point defect reactions and dynamics is aggravated by the complex incorporation and defect interaction behavior of C in group-III nitrides. Carbon preferentially substitutes nitrogen atoms (acceptor type) [8,9], but can also incorporate on gallium lattice sites (donor type), leading to self-compensation [10,11]. Additionally, numerous interstitial sites and complexes [9–13], some involving multiple carbon atoms [9,14–16], further complicate the defect landscape. Furthermore, calculations of formation energies and charge transfer levels point to vastly opposing effects of C on the different incorporation sites on the electronic properties of, e.g., GaN. Hence, the relative occurrence of the different incorporation sites and the dynamic switching processes between them become a delicate

Published by the American Physical Society under the terms of the Creative Commons Attribution 4.0 International license. Further distribution of this work must maintain attribution to the author(s) and the published article's title, journal citation, and DOI.

and highly sensitive ingredient in understanding the effect of C impurities.

In this paper we investigate C point defect reactions and quantify their dynamics by probing the time and temperature dependence of the Fermi-level pinning upon annealing using electron holography (EH) in a transmission electron microscope (TEM). We identify that the atomic process lifting the Fermi-level pinning in C-implanted GaN has a jump length in the range of a single lattice constant and a charge reversal in line with a site switching of C from substitutional to interstitial sites. The process has an activation barrier energy of 2.27 ± 0.26 eV. Our work demonstrates the application of EH in identifying and quantifying point defect reactions in GaN, shedding light on their dynamics and crucial implications for semiconductor device stability.

II. SAMPLE AND METHODS

As a model system, we used thin lamellas extracted from a silicon-doped n-n⁺ GaN junction grown by MOVPE on a c-plane freestanding GaN substrate with a low dislocation density of $\sim 1 \times 10^6$ cm⁻². The doping levels in the *n* and n^+ layers are 8×10^{17} and 3.5×10^{18} cm⁻³, respectively, as determined by secondary ion mass spectrometry (SIMS). The thin lamellas are prepared using focused ion beam (FIB) milling in a FEI Helios NanoLab 400S instrument. The final FIB polishing is performed at 5 keV with an ion dose rate of 16 pA at an incident angle of 5°. Due to the usage of C-containing protective layers as well as the hydrocarbon contamination inside the FIB chamber, the FIB preparation dominantly implants C in the surface region of the lamellas. Transport and range of ions in matter (TRIM) simulations [17] taking into account the experimental conditions, reveal an exponentially decaying C implantation profile with concentrations above the doping level extending $\sim \! \! 15 \text{ nm}$ into the lamellas (see Fig. S4 and further experimental details in Supplemental Material [18]) [19,20].

The such prepared lamellas are investigated by off-axis electron holography inside a TEM (FEI Titan G2 60-300

^{*}Contact author: p.ebert@fz-juelich.de

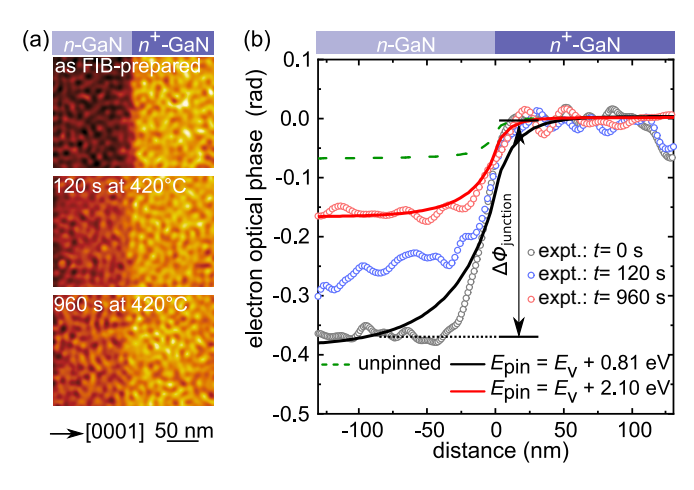


FIG. 1. (a) Electron optical phase maps of the n-n⁺ GaN junction measured by electron holography in TEM. The top figure illustrates the phase distribution of an as-FIB-prepared TEM lamella, whereas the middle and bottom figures were acquired after annealing at 420 °C for 120 and 960 s, respectively. (b) Corresponding line profiles revealing the change of the electron optical phase across the n-n⁺ GaN junction upon annealing at 420 °C (open symbols). The junction interface is located at 0 nm spatial position. The lines represent simulations of the phase profile for different pinning levels at the surface of the TEM lamella. The lowest pinning level in the as-FIB-prepared state is attributed to FIB-implanted C_N , whereas the higher one after annealing arises from the states at the amorphous-crystalline interface near the surface of the TEM lamella. For phase profiles acquired under different temperatures, see Supplemental Material [18].

HOLO, FEI instrument) operated at 300 kV at a dose rate of 30 $e/(\text{nm}^2 \text{ s})$ [21]. For the given electron dose rate and acceleration voltage, the phase contrast across the n-n⁺ GaN junctions remains constant at room temperature for at least 4 h (cf. Fig. S3 in Supplemental Material [18]), indicating that irradiation damage will not affect the experimental results. *In situ* annealing was performed using a double-tilt Gatan model 652 heating holder, while the gun valve was closed.

The electron optical phase derived from the holograms provides the electrostatic potential averaged along the electron beam direction. Hence, the screening of the surface potential arising from the Fermi-level pinning (due to near surface C implantation) changes the average potential and thus the electron optical phase. In return, one can derive quantitatively the change in Fermi-level pinning position upon annealing from the changes in the electron optical phase with the help of a self-consistent electrostatic simulation [19,22].

III. RESULTS

Figure 1(a) illustrates the evolution of electron optical phase maps acquired at an n-n⁺ GaN junction upon annealing at 420 °C. It can be observed that the phase contrast between the n and n⁺ GaN layers reduces with annealing time. To quantify these changes induced by annealing, we extract phase profiles from measured electron optical phase maps averaged over a width of 400 nm. Figure 1(b) depicts examples of the derived phase profiles (symbols) acquired after successive

annealing at 420 °C for different times. Before annealing, in the as-FIB-prepared state, the lateral change of the phase across the n-n⁺ GaN junction has the shape of a broadened step function with a height, i.e., phase step $\Delta\phi_{\rm junction}$ of 0.37 rad [see Fig. 1(a)]. Upon annealing $\Delta\phi_{\rm junction}$ becomes smaller, reducing to 0.26 rad after 120 s and finally to 0.17 rad after 960 s annealing. Additional annealing no longer results in a further change of $\Delta\phi_{\rm junction}$, suggesting that the healing process is terminated.

For a quantitative understanding of the decrease in $\Delta \phi_{\text{iunction}}$ with annealing, we performed a self-consistent electrostatic simulation of the phase across the junction, as described in Refs. [19,22] and in the Supplemental Material Sec. 7 [18]. The presence of an amorphous outer shell at the surface, as well as a FIB-induced defect-rich inner shell in the crystalline part below the outer shell, will induce states in the band gap, leading to pinning of the Fermi level [19,22]. We model the pinning using a Gaussian distribution of surface states integrated from the charge neutrality level to the Fermi level. The resulting two-dimensional (2D) sheet charge is localized at the interface between the amorphous outer shell and the pristine crystalline core [19]. The calculated electrostatic potential (see Fig. S6 in the Supplemental Material [18]) is used to derive the phase profiles across the n-n⁺ GaN junction for different surface Fermi-level pinnings (E_{pin}) . The green dashed line in Fig. 1(b) yields the phase profile calculated for a TEM lamella without surface pinning (i.e., being unpinned). The "unpinned" phase step is smaller than any of the measured ones at any annealing stage. Hence, the TEM lamella cannot be unpinned near its surfaces. The best-fitting simulation results for the as-prepared and fully healed TEM lamellas are shown as solid lines in Fig. 1(b). Note, the surface Fermilevel pinning-increased phase step across the junction is due to the doping level-dependent screening length of the near surface electrostatic potential (induced by the pinning) [22].

The simulation yields the following Fermi-level pinnings: (i) In the as-FIB-prepared state, we found an averaged surface Fermi-level pinning of (0.57 ± 0.13) eV above the valence band edge (E_V) . This pinning level value is consistent with previous experimental values and is compatible only with the (0/-) charge transfer level of carbon substitutionals on nitrogen sites (C_N) [19] which has been calculated to be around 0.8 eV above E_V [8,9,13,23,24]. All other intrinsic defects [25,26] and possible FIB-implanted impurities (e.g., Pt [27]), as well as carbon-related complex defects [9,14], do not exhibit appropriate acceptor-type charge transfer levels in the vicinity of the measured Fermi-level pinning energy (see Supplemental Material Sec. 6 [18] for an in-depth discussion about C_N as the electrically dominating point defect).

(ii) After termination of the thermal healing process (e.g., 960 s and longer annealing) the pinning level increases to $E_V + (2.14 \pm 0.09)$ eV. This midgap pinning level is attributed to the states present at the amorphous shell-crystalline core interface of the TEM lamella [19,22].

At this stage, we address the temporal evolution of $\Delta\phi_{\rm junction}$ upon annealing time: Figure 2(a) illustrates the decay of $\Delta\phi_{\rm junction}$ versus annealing time t for four lamellas, each subjected to a different annealing temperature T (colored symbols). For all data sets, the phase step is between 0.37 and 0.45 rad in the as-FIB-prepared state. Annealing leads to an

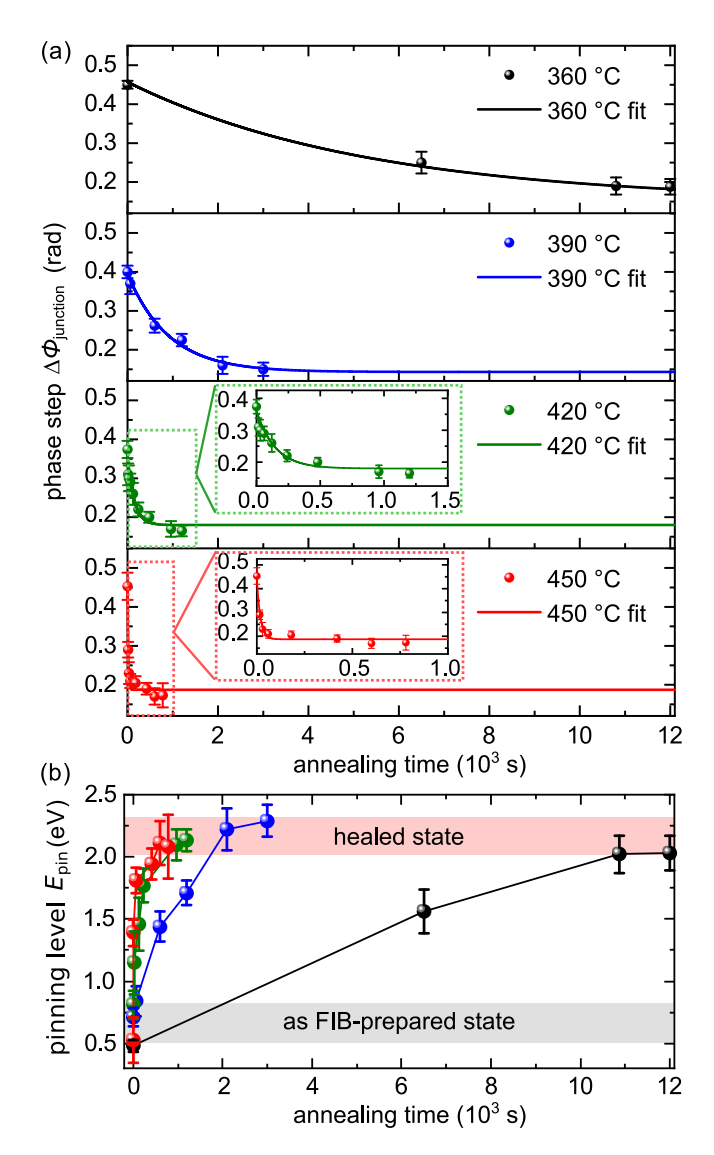


FIG. 2. (a) Time evolution of the phase step $\Delta\phi_{\rm junction}$ across the n-n⁺ GaN junction for different annealing temperatures. (b) Derived pinning levels of the Fermi energy at the surface of the TEM lamellas vs annealing time. The data reveal a shift of the average pinning from $E_{\rm V}+(0.57\pm0.13)~{\rm eV}$, attributed to carbon impurities on nitrogen sites (as-FIB-prepared state), to $E_{\rm V}+(2.14\pm0.09)~{\rm eV}$, attributed to the states at the amorphous outer shell–crystalline core interface (healed state).

exponential decay of $\Delta\phi_{\rm junction}$, which approaches asymptotically a saturation value, ranging between 0.15 and 0.18 rad. The time required to reach the saturation value strongly decreases with temperature.

The time dependence of $\Delta \phi_{\text{junction}}$ can be described in first approximation by an exponential decay,

$$\Delta \phi_{\text{junction}}(t, T) = \Delta \phi_0 \exp\left(-\frac{t}{\tau(T)}\right) + \Delta \phi_{\infty}$$
 (1)

where $\Delta\phi_{\infty}$ is the saturation value after complete healing, and $\Delta\phi_0 + \Delta\phi_{\infty}$ is the phase step at the junction in the as-FIB-prepared state. $\tau(T)$ is the temperature-dependent time constant of the healing process. For each temperature, an exponential fit of measured $\Delta\phi_{\mathrm{junction}}(t)$ values is shown as solid

TABLE I. Time constant (τ) obtained from the exponential fit to the electron optical phase step across the n-n⁺ GaN junctions for different annealing temperatures.

<i>T</i> (°C)	Time constant τ (s)	
360 390 420 450	$5308^{+1483}_{-1443} \\ 912^{+197}_{-157} \\ 147^{+68}_{-28} \\ 18^{+44}_{-4}$	

line. For data sets acquired at 420 and 450 °C enlarged insets are added for better visibility of the decay. The physically most relevant parameter is the time constant $\tau(T)$. Table I provides the values of $\tau(T)$ obtained for different annealing temperatures.

In order to identify the time constants' physical background, we first relate the decay of $\Delta\phi_{\rm junction}$ with the surface Fermi-level pinning. For this purpose, we simulated all phase profiles and show in Fig. 2(b) the evolution of the derived pinning levels as a function of time and temperature. The values reveal an exponential convergence from pinning levels of $E_{\rm V}+(0.57\pm0.13)~{\rm eV}$ towards $E_{\rm V}+(2.14\pm0.09)~{\rm eV}$ after extended annealing.

We recall that the lower pinning value is assigned to $C_{\rm N}$ defects implanted during FIB preparation, whereas the higher pinning level is assigned to the presence of the interface between the amorphous outer shell and the crystalline core [19]. The latter cannot be healed thermally at the low temperatures used and remains even after healing.

C_N defects pin the Fermi level if their concentration is sufficiently above the doping concentration. Lowering the C_N concentration will gradually shift the pinning from being C_N dominated to being dominated by the states at the amorphouscrystalline interface. Hence, the shift in pinning levels reflects the reduction of the concentration of C_N. In first approximation, this reduction in C_N concentration can be described as a thermal migration process. Once the C_N concentration is sufficiently below the doping concentration, carbon becomes electrically irrelevant. Hence, the time constant $\tau(T)$ of the $\Delta\phi_{\text{junction}}$ decay reflects the time needed to reduce the C_{N} concentration sufficiently below the doping concentration. Since we always used exactly the same FIB preparation procedure we expect a consistent C implantation depth and concentration for each lamella. Thus, the diffusion length L required for the C_N concentration to fall significantly below the doping concentration and thus be electrically irrelevant, can be anticipated to be a constant and temperature-independent value given by

$$L = \sqrt{D(T)\tau(T)} = \text{const.}$$
 (2)

D(T) is a temperature-dependent diffusion coefficient [25]

$$D(T) = D_0 \exp\left(-\frac{E_b}{k_B T}\right),\tag{3}$$

where D_0 is the preexponential factor dependent on geometry and crystal structure. E_b is the activation barrier energy and k_B is the Boltzmann constant. Inserting Eq. (3) into Eq. (2) yields

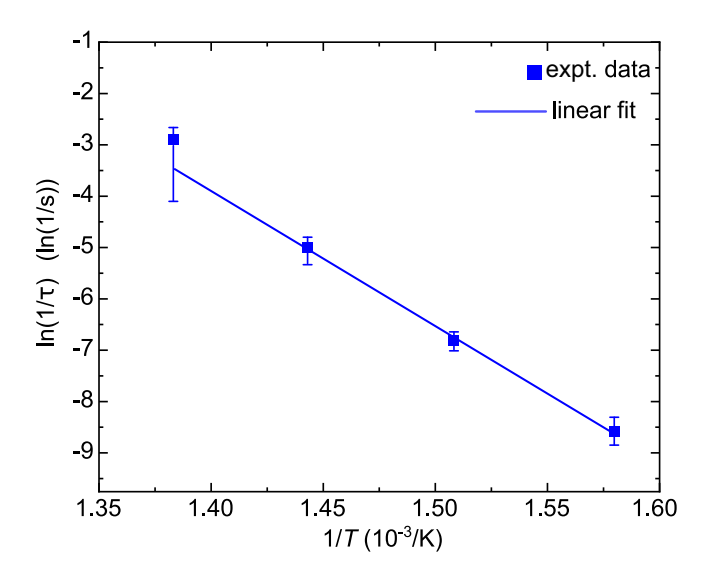


FIG. 3. Arrhenius plot of the measured $\ln(1/\tau)$ values vs 1/T. The line represents a linear fit according to Eq. (4). The slope yields an activation barrier energy $E_{\rm b}=2.27\pm0.26$ eV.

an Arrhenius equation:

$$\ln\left(\frac{1}{\tau}\right) = \ln\left(\frac{D_0}{L^2}\right) - \left(\frac{E_b}{k_B}\right)\frac{1}{T}.\tag{4}$$

Figure 3 depicts the logarithm of the inverse time constant $1/\tau$ derived from the exponential decay of $\Delta\phi_{\rm junction}$ in Fig. 2(a) versus inverse temperature (1/T). The data exhibit a linear relation in accordance with Eq. (4). The slope of the linear fit (blue line) yields an activation barrier energy $E_{\rm b} = 2.27 \pm 0.26$ eV.

The intercept of the Arrhenius plot is found to be

$$\ln(D_0/L^2) = (32.9 \pm 4.5) \ln(1/s). \tag{5}$$

According to Eq. (4) the intercept is related to the diffusion length L. The preexponential factor D_0 is given by ga^2v , where a is the (in-plane) lattice constant, v the attempt frequency, and g the geometry factor [25]. The geometry factor depends on the crystal structure and exact diffusion path(s) and can be approximated to be in the order of one [28]. The attempt frequency is approximated by the frequency, where the phonons of nitrogen atoms have the highest density of states, i.e., $\sim 1.6 \times 10^{13} \text{ s}^{-1}$ [29]. We obtain a diffusion length after a time of 3τ (at which full healing is achieved) of $(0.28^{+2.40}_{-0.25})a$. This points to a single atomic jump process being responsible for lifting the Fermi-level pinning induced by C_N .

IV. DISCUSSION

To understand the measured activation barrier energy and small diffusion length, we need to address the atomic mechanisms related to carbon point defects during annealing. Therefore, we recall that before annealing the surface of the as-FIB-prepared lamella is pinned at $\sim E_V + 0.57$ eV, which is attributed to the singly negatively charged C_N^- [19]. During annealing this pinning level vanishes, leading to an upward shift of the Fermi level pinning. One possible explanation for

this behavior would be the diffusion of C_N^- from the surface towards the crystalline bulk and/or the amorphous outer shell, effectively reducing the C_N^- concentration below the doping concentration.

 ${\rm C_N}^-$ diffusion can be realized via nitrogen vacancies. The nitrogen vacancy has, however, a rather high migration barrier of ${\sim}4$ eV for the ${+}1e$ charge state at the given Fermi-level position [25,30]. Thus, vacancy mediated migration of substitutional C can be ruled out.

Alternatively, diffusion can take place through carbon interstitials, which can be created by atomic kick-out or a switching process. The activation barrier energy for this diffusion process has been calculated to be strongly affected by the charge state of C_i and, consequently, by the surface Fermi-level position, spanning from 1.6, 2.4, to 3.0 eV for C_i^{2+} , C_i^+ , to C_i^0 , respectively [30].

However, interstitial diffusion is actually not needed for lifting the Fermi-level pinning near the valence band edge, since with a substitutional to interstitial site switch of C, the presence of (0/-) charge transfer levels in the lower part of the band gap vanish (C_i have no such charge transfer levels): Upon site switch from the substitutional onto an interstitial site the charge of carbon changes from negative to positive [30] and thereby carbon becomes electrically inactive already (for n-type GaN and in the presence of a further midgap pinning, e.g., at the amorphous-crystalline interface). In addition, once switched, the positively charged C_i experiences a repulsive Coulomb interaction with the newly formed positively charged N vacancy, effectively blocking a back jump. Hence, a single site switch is sufficient.

This is in line with our measurements: First, classical carbon outdiffusion would require a diffusion length well above 10 nm since the C implantation profile at the given energy is expected to have a width of \sim 15 nm [19]. Hence, the experimentally obtained diffusion length in the order of one atomic jump distance is rather consistent with a C site switching process. Therefore, the experimentally obtained activation barrier energy of 2.27 ± 0.26 eV is attributed to the energy barrier of the carbon site switching process from substitutional to interstitial.

On the basis of the above results, one can estimate the thermal stability of C-doped semi-insulating GaN layers in, e.g., HEMTs, since the C site switch would remove the deep level in the lower part of the band gap responsible for achieving insulating properties. We anticipate that continuous operation at a maximum temperature of approximately 220 °C can be sustained over a 20-year period.

V. CONCLUSIONS

In summary, we quantified the dynamics of C-implanted defects in GaN upon annealing by probing the Fermi-level changes using off-axis electron holography. We identify that switching of C from substitutional to interstitial sites is the atomic process responsible for lifting the Fermi-level pinning in the lower part of the band gap and hence for removing the semi-insulating properties of C-doped GaN insulating layers. This site switching process has an activation barrier energy of 2.27 ± 0.26 eV, providing a quantitative access to device

degradation. In addition, our work establishes electron holography in a TEM as a methodology to probe the dynamics and reactions of time-resolved point defects and assess the thermal physical processes governing semiconductor device stability. This overshadows prior applications of EH mapping potential and charge distributions [22,31–41] and inferring the presence of point defects [19,42,43] in a range of semiconductor materials, nanostructures, and devices.

ACKNOWLEDGMENTS

The authors thank D. S. Rosenzweig for helpful discussions and the AIDAS project - AI, Data Analytics and Scalable Simulation, France - which is a Joint Virtual Laboratory gathering the Forschungszentrum Jülich (FZJ) and the French Alternative Energies and Atomic Energy Commission (CEA) for financial support.

- [1] P. Perlin, L. Marona, M. Leszczynski, T. Suski, P. Wisniewski, R. Czernecki, and I. Grzegory, Degradation mechanisms of InGaN laser diodes, Proc. IEEE 98, 1214 (2010).
- [2] L. Marona, P. Wisniewski, P. Prystawko, I. Grzegory, T. Suski, S. Porowski, P. Perlin, R. Czernecki, and M. Leszczyński, Degradation mechanisms in InGaN laser diodes grown on bulk GaN crystals, Appl. Phys. Lett. 88, 201111 (2006).
- [3] E. A. Jones, F. Wang, and B. Ozpineci, Application-based review of GaN HFETs, in 2014 IEEE Workshop on Wide Bandgap Power Devices and Applications (IEEE, New York, 2014), pp. 24–29.
- [4] A. Armstrong, A. R. Arehart, B. Moran, S. P. DenBaars, U. K. Mishra, J. S. Speck, and S. A. Ringel, Impact of carbon on trap states in *n*-type GaN grown by metalorganic chemical vapor deposition, Appl. Phys. Lett. 84, 374 (2004).
- [5] P. Gamarra, C. Lacam, M. Tordjman, J. Splettstösser, B. Schauwecker, and M.-A. di Forte-Poisson, Optimisation of a carbon doped buffer layer for AlGaN/GaN HEMT devices, J. Cryst. Growth 414, 232 (2015).
- [6] M. J. Uren, M. Silvestri, M. Cäsar, G. A. M. Hurkx, J. A. Croon, J. Šonský, and M. Kuball, Intentionally carbon-doped AlGaN/GaN HEMTs: Necessity for vertical leakage paths, IEEE Electron Device Lett. 35, 327 (2014).
- [7] N. Remesh, N. Mohan, S. Raghavan, R. Muralidharan, and D. N. Nath, Optimum carbon concentration in GaN-on-silicon for breakdown enhancement in AlGaN/GaN HEMTs, IEEE Trans. Electron Devices 67, 2311 (2020).
- [8] J. L. Lyons, A. Janotti, and C. G. Van de Walle, Carbon impurities and the yellow luminescence in GaN, Appl. Phys. Lett. 97, 152108 (2010).
- [9] M. Matsubara and E. Bellotti, A first-principles study of carbon-related energy levels in GaN. I. Complexes formed by substitutional/interstitial carbons and gallium/nitrogen vacancies, J. Appl. Phys. 121, 195701 (2017).
- [10] A. F. Wright, Substitutional and interstitial carbon in wurtzite GaN, J. Appl. Phys. 92, 2575 (2002).
- [11] C. H. Seager, A. F. Wright, J. Yu, and W. Götz, Role of carbon in GaN, J. Appl. Phys. 92, 6553 (2002).
- [12] J. L. Lyons, A. Janotti, and C. G. Van de Walle, Effects of carbon on the electrical and optical properties of InN, GaN, and AlN, Phys. Rev. B **89**, 035204 (2014).
- [13] P. Deák, M. Lorke, B. Aradi, and T. Frauenheim, Carbon in GaN: Calculations with an optimized hybrid functional, Phys. Rev. B **99**, 085206 (2019).
- [14] J. L. Lyons, E. R. Glaser, M. E. Zvanut, S. Paudel, M. Iwinska, T. Sochacki, and M. Bockowski, Carbon complexes in highly C-doped GaN, Phys. Rev. B 104, 075201 (2021).

- [15] D. O. Demchenko, I. C. Diallo, and M. A. Reshchikov, Hydrogen-carbon complexes and the blue luminescence band in GaN, J. Appl. Phys. 119, 035702 (2016).
- [16] F. Zimmermann, J. Beyer, F. C. Beyer, G. Gärtner, I. Gamov, K. Irmscher, E. Richter, M. Weyers, and J. Heitmann, A carbon-doping related luminescence band in GaN revealed by below bandgap excitation, J. Appl. Phys. 130, 055703 (2021).
- [17] J. F. Ziegler, M. D. Ziegler, and J. P. Biersack, SRIM the stopping and range of ions in matter (2010), Nucl. Instrum. Methods Phys. Res. B 268, 1818 (2010).
- [18] See Supplemental Material at http://link.aps.org/supplemental/ 10.1103/PhysRevResearch.7.013200 for details about the TEM lamella preparation process using FIB, the crystalline and overall thicknesses of the FIB-prepared lamellas, experimental details (minimization of dynamic contrast and beam induced damage), electrostatic- and TRIM simulations, as well as the identification of C_N as the electrically dominating point defect.
- [19] K. Ji, M. Schnedler, Q. Lan, F. Zheng, Y. Wang, Y. Lu, H. Eisele, J.-F. Carlin, R. Butté, N. Grandjean, R. E. Dunin-Borkowski, and Ph. Ebert, Identification and thermal healing of focused ion beam-induced defects in GaN using off-axis electron holography, Appl. Phys. Express 17, 016505 (2024).
- [20] Probing low C concentrations in the first 10 nm below a surface is a delicate task with present analytical techniques: On the one hand, the large C surface contaminations blur the depth resolutions of, e.g., SIMS, covering the signal of the subsurface A atoms. On the other hand, the concentration of the subsurface Catoms is too low to be probed by, e.g., atom probe tomography. Energy-dispersive x-ray spectroscopy integrates over the whole sample including the surface contamination. Cleaning the C surface contamination by, e.g., plasma cleaning, annealing, sputtering, etc., would initiate C mobility and thus alter the as-prepared subsurface C profile or remove the near surface layers and thereby the subsurface C. Hence, we chose to tackle the issue indirectly by TRIM calculations later on corroborated by combining the measured charge transfer level with density functional calculations.
- [21] C. Boothroyd, A. Kovács, and K. Tillmann, FEI Titan G2 60-300 HOLO, J. Large-Scale Res. Facil. 2, A44 (2016).
- [22] Y. Wang, M. Schnedler, Q. Lan, F. Zheng, L. Freter, Y. Lu, U. Breuer, H. Eisele, J.-F. Carlin, R. Butté, N. Grandjean, R. E. Dunin-Borkowski, and Ph. Ebert, Interplay of anomalous strain relaxation and minimization of polarization changes at nitride semiconductor heterointerfaces, Phys. Rev. B 102, 245304 (2020).

- [23] M. A. Reshchikov, D. O. Demchenko, A. Usikov, H. Helava, and Y. Makarov, Carbon defects as sources of the green and yellow luminescence bands in undoped GaN, Phys. Rev. B 90, 235203 (2014).
- [24] D. O. Demchenko, I. C. Diallo, and M. A. Reshchikov, Yellow luminescence of gallium nitride generated by carbon defect complexes, Phys. Rev. Lett. 110, 087404 (2013).
- [25] S. Limpijumnong and C. G. Van de Walle, Diffusivity of native defects in GaN, Phys. Rev. B **69**, 035207 (2004).
- [26] J. L. Lyons and C. G. Van de Walle, Computationally predicted energies and properties of defects in GaN, npj Comput. Mater. 3, 12 (2017).
- [27] D.-H. Yeh, L.-Z. Hsieh, L.-B. Chang, and M.-J. Jeng, The characteristics of platinum diffusion in *n*-type GaN, Appl. Surf. Sci. **253**, 6910 (2007).
- [28] J. R. Manning, Diffusion Kinetics for Atoms in Crystals (Van Nostrand, Princeton, NJ, 1968).
- [29] D.-S. Tang and L.-M. Zhang, Phonon modes and topological phonon properties in (GaN)_x/(Aln)_x and (AlGaN)_x/(GaN)_x superlattices, Phys. Scr. **98**, 085934 (2023).
- [30] A. Kyrtsos, M. Matsubara, and E. Bellotti, Migration mechanisms and diffusion barriers of carbon and native point defects in GaN, Phys. Rev. B **93**, 245201 (2016).
- [31] W. D. Rau, P. Schwander, F. H. Baumann, W. Höppner, and A. Ourmazd, Two-dimensional mapping of the electrostatic potential in transistors by electron holography, Phys. Rev. Lett. **82**, 2614 (1999).
- [32] A. C. Twitchett, R. E. Dunin-Borkowski, and P. A. Midgley, Quantitative electron holography of biased semiconductor devices, Phys. Rev. Lett. 88, 238302 (2002).
- [33] M. Beleggia, P. F. Fazzini, P. G. Merli, and G. Pozzi, Influence of charged oxide layers on TEM imaging of reverse-biased *p-n* junctions, Phys. Rev. B **67**, 045328 (2003).
- [34] D. Cooper, A. C. Twitchett, P. K. Somodi, P. A. Midgley, R. E. Dunin-Borkowski, I. Farrer, and D. A. Ritchie, Improvement in electron holographic phase images of focused-ion-beam-milled

- GaAs and Si *p-n* junctions by in situ annealing, Appl. Phys. Lett. **88**, 063510 (2006).
- [35] C. Gatel, R. Serra, K. Gruel, A. Masseboeuf, L. Chapuis, R. Cours, L. Zhang, B. Warot-Fonrose, and M. J. Hÿtch, Extended charge layers in metal-oxide-semiconductor nanocapacitors revealed by *Operando* electron holography, Phys. Rev. Lett. 129, 137701 (2022).
- [36] J. Cumings, A. Zettl, M. R. McCartney, and J. C. H. Spence, Electron holography of field-emitting carbon nanotubes, Phys. Rev. Lett. **88**, 056804 (2002).
- [37] C. Gatel, A. Lubk, G. Pozzi, E. Snoeck, and M. Hÿtch, Counting elementary charges on nanoparticles by electron holography, Phys. Rev. Lett. **111**, 025501 (2013).
- [38] Y. Yao, C. Li, Z. L. Huo, M. Liu, C. X. Zhu, C. Z. Gu, X. F. Duan, Y. G. Wang, L. Gu, and R. C. Yu, *In situ* electron holography study of charge distribution in high-κ charge-trapping memory, Nat. Commun. 4, 2764 (2013).
- [39] S. Toyama, T. Seki, Y. Kanitani, Y. Kudo, S. Tomiya, Y. Ikuhara, and N. Shibata, Real-space observation of a two-dimensional electron gas at semiconductor heterointerfaces, Nat. Nanotechnol. 18, 521 (2023).
- [40] X. Xu, Y. Liu, J. Wang, D. Isheim, V. P. Dravid, C. Phatak, and S. M. Haile, Variability and origins of grain boundary electric potential detected by electron holography and atom-probe tomography, Nat. Mater. 19, 887 (2020).
- [41] D. Cherns and C. G. Jiao, Electron holography studies of the charge on dislocations in GaN, Phys. Rev. Lett. 87, 205504 (2001).
- [42] Y. Lu, F. Zheng, Q. Lan, M. Schnedler, P. Ebert, and R. E. Dunin-Borkowski, Counting point defects at nanoparticle surfaces by electron holography, Nano Lett. 22, 6936 (2022).
- [43] Q. Lan, C. Wang, L. Jin, M. Schnedler, L. Freter, K. Fischer, J. Caron, X.-K. Wei, T. Denneulin, A. Kovács, P. Ebert, X. Zhong, and R. E. Dunin-Borkowski, Electrostatic shaping of magnetic transition regions in La_{0.7}Sr_{0.3}MnO₃, Phys. Rev. Lett. 129, 057201 (2022).